ADVANCED INTELLIGENT SYSTEMS
Open Access
www.advintellsyst.com

Biodegradable and Flexible Polymer-Based Memristor Possessing Optimized Synaptic Plasticity for Eco-Friendly Wearable Neural Networks with High Energy Efficiency

*Sungjun Oh, Hyungjin Kim, Seong Eun Kim, Min-Hwi Kim, Hea-Lim Park, and Sin-Hyung Lee**

Organic memristors are promising candidates for the flexible synaptic components of wearable intelligent systems. With heightened concerns for the environment, considerable effort has been made to develop organic transient memristors to realize eco-friendly flexible neural networks. However, in the transient neural networks, achieving flexible memristors with biorealistic synaptic plasticity for energy efficient learning processes is still challenging. Herein, a biodegradable and flexible polymer-based memristor, suitable for the spike-dependent learning process, is demonstrated. An electrochemical metallization phenomenon for the conductive nanofilament growth in a polymer medium of poly (vinyl alcohol) (PVA) is analyzed and a PVA-based transient and flexible artificial synapse is developed. The developed device exhibits superior biodegradability and stable mechanical flexibility due to the high water solubility and excellent tensile strength of the PVA film, respectively. In addition, the developed flexible memristor is operated as a reliable synaptic device with optimized synaptic plasticity, which is ideal for artificial neural networks with the spike-dependent operations. The developed device is found to be effectively served as a reliable synaptic component with high energy efficiency in practical neural networks. This novel strategy for developing transient and flexible artificial synapses can be a fundamental platform for realizing eco-friendly wearable intelligent systems. An interactive preprint version of the article can be found here: https://doi.org/10.22541/au.166603245.58711630/v1.

1. Introduction

Flexible neuromorphic electronics for the computing systems of smart wearable electronics have attracted great attention because of their merits in terms of energy efficiency and operating speed.[1–3] In practical hardware neural networks, a memory device completely mimicking a biological synapse is a crucial component in achieving energy-efficient operations.[1,4–6] An organic material-based resistive switching device, i.e., an organic memristor, has been considered as a favorable memory component of flexible neuromorphic systems, in the viewpoints of mechanical flexibility and synaptic functionality.[3,7–9] Thus far, diverse mechanisms for the resistive switching of organic memristors have been explored, such as ion migration,[10] ferroelectricity,[11] and electrochemical metallization (ECM).[3,12–14] Among the various types of organic memristors, ECM-based devices have been demonstrated as promising artificial synapses of practical systems owing to their great scalability and superior electrical characteristics.[13,14] For organic

S. Oh, S. E. Kim, S.-H. Lee
School of Electronics Engineering
Kyungpook National University
80 Daehak-ro, Buk-gu, Daegu 702-701, Republic of Korea
E-mail: sinhlee@knu.ac.kr, jls87@snu.ac.kr

S. Oh, S. E. Kim, S.-H. Lee
School of Electronic and Electrical Engineering
Kyungpook National University
80 Daehak-ro, Buk-gu, Daegu 702-701, Republic of Korea

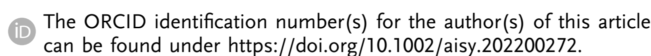
The ORCID identification number(s) for the author(s) of this article can be found under https://doi.org/10.1002/aisy.202200272.

© 2022 The Authors. Advanced Intelligent Systems published by Wiley-VCH GmbH. This is an open access article under the terms of the Creative Commons Attribution License, which permits use, distribution and reproduction in any medium, provided the original work is properly cited.

DOI: 10.1002/aisy.202200272

H. Kim
Department of Materials Science and Engineering
Yonsei University
Seoul 03722, Republic of Korea

M.-H. Kim
School of Electrical and Electronics Engineering
Chung-Ang University
Seoul 06974, Republic of Korea

H.-L. Park
Department of Materials Science and Engineering
Seoul National University of Science and Technology
Seoul 01811, Republic of Korea

ECM memristors, a nanoscale metallic conductive filament (CF) is formed or ruptured in an organic medium under an electric stimulus, resulting in the resistive switching characteristics of such devices. Because the CF growth is mainly governed by the distribution of the electric field in an ECM memristor, the multilevel resistance states can be obtained by controlling the conditions of the electric stimulus.[3,13] In addition, the stability of the CF is dependent on its structure, and thus short-term plasticity (STP) and long-term plasticity (LTP) of biological synapses can be mimicked in the ECM device by precisely controlling the CF dynamics.[15,16] Recently, the development of transient electronics with biodegradable and biocompatible characteristics has been urgently needed as environmental concerns increased.[17,18] To realize the eco-friendly practical neuromorphic systems with high energy efficiency, it is important to achieve the spike-dependent learning process in the transient artificial synapse. For such operations, the synaptic device with bio-realistic synaptic plasticity is an essential component. Specifically, the artificial synapse should possess the STP and LTP characteristics for training on different time scales of successive electric stimuli through a combination of STP and LTP.[19] Additionally, for compatibility with other neuromorphic components, the diverse time windows for synaptic plasticity should be obtained in the synapse devices.[8] Although several studies on the biomaterial-based ECM memristors with transient features have been conducted,[20–30] it is still challenging to achieve bio-realistic synaptic devices with biodegradability and flexibility, due to the difficulties in controlling the CF dynamics.

Poly(vinyl alcohol) (PVA) with high water solubility is a promising polymer for biodegradable films.[31,32] It is widely utilized as an insulator in flexible electronics because of its excellent mechanical flexibility and superior electrical characterizations.[33,34] Despite such functionalities of PVA for transient and flexible electronics, the ECM phenomenon, essential for the CF growth, has not been reported in the pure PVA medium yet. Previously, PVA has not been regarded as a medium, suitable for the ECM memristor, and it has been used as an insulator for the memristors based on the ion migration[35–37] or the dipole alignment,[38] and a matrix of an ion-doped electrolyte.[39] In such devices, only the limited synaptic function (STP or LTP) was demonstrated owing to the inherent characteristics in the switching mechanism (see Table S1, Supporting Information). Specifically, for the CF-based memristor consisting of the ion-doped PVA matrix, the constant ion density restricted the synaptic function to LTP.[39] In the memristors based on the ion-doped electrolytes, it is difficult to achieve both the LTP and STP functions because the metal ion density is governed by the doping concentration, not the electric stimuli applied to the devices.[40,41] For realizing the eco-friendly wearable neural networks with high energy efficiency, it is important to develop the transient ECM memristor with mechanical flexibility and optimized synaptic plasticity for the spike-dependent learning.

In this work, we developed a PVA-based ECM memristor with optimized synaptic plasticity for a transient artificial synapse of an eco-friendly flexible neural network with high energy efficiency, as shown in **Figure 1**a. The resistive switching effects attributed to the metallic CF formation in the PVA media with different molecular weights (M_w) were analyzed. When the M_w value of the polymer medium is sufficiently low, the resistive switching behaviors based on the ECM phenomenon were effectively achieved, and the memory stability and time windows for synaptic plasticity were found to be effectively tuned by the

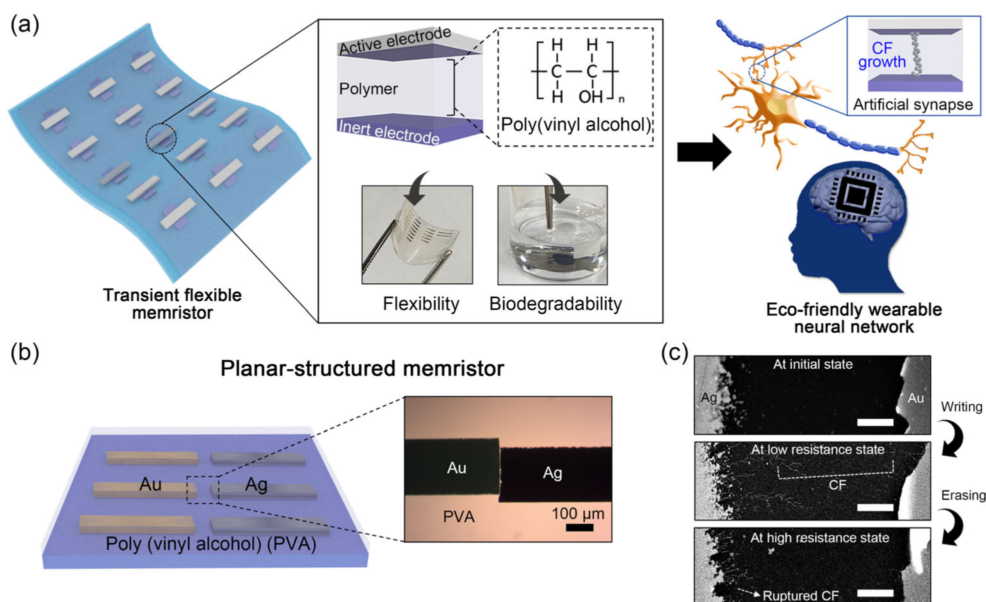

Figure 1. Dynamics of the metallic conductive filament growth in the poly (vinyl alcohol) (PVA)-based memristor. a) Schematics presenting the structure of the PVA-based memristor with mechanical flexibility and biodegradability, and its potentials as an artificial synapse for hardware-based eco-friendly neural networks. b) A schematic showing the PVA-based memristors with a planar structure. Three types of the devices with the different polymer molecular weights (M_ws) (130 000, 23 000, and 10 000 g mol^{-1}) were prepared. An inset image shows a microscopic photograph of the device. c) Active surfaces of the device according to the resistance states. Each surface was investigated using a field-emission scanning electron microscope (scale bar, 1 μm).

 © 2022 The Authors. Advanced Intelligent Systems published by Wiley-VCH GmbH

26404567, 0, Downloaded from https://onlinelibrary.wiley.com/doi/10.1002/aisy.202200272 by Chung-Ang University, Wiley Online Library on [27/03/2023]. See the Terms and Conditions (https://onlinelibrary.wiley.com/terms-and-conditions) on Wiley Online Library for rules of use; OA articles are governed by the applicable Creative Commons License

polymer M_w. On the basis of the understanding of the ECM phenomenon in the polymer medium of PVA, we fabricated a PVA-based flexible memristor with biodegradable characteristics and optimized its synaptic plasticity. The developed memristor exhibited stable nonvolatile memory characteristics during successive mechanical stresses, and it was swiftly dissolved in deionized (DI) water. Moreover, synaptic characteristics for neuromorphic systems including STP, LTP, paired-pulse facilitation (PPF), spike-number-dependent plasticity (SNDP), and spike-rate-dependent plasticity (SRDP) were successfully demonstrated in the developed device. The hardware neural networks based on the device showed the reliable logic operations with high energy efficiency. In the SPICE simulation, the device showed the great potentials for realizing practical artificial neural networks.

2. Results and Discussion

We first analyzed the ECM phenomenon for the metallic CF growth in the PVA medium. Three types of planar-structured memristors consisting of PVA insulator with the different $M_w s$ (10 000, 23 000, and 130 000 g mol^{-1}) were fabricated as shown in Figure 1b. Active and inert electrodes were prepared using silver and gold, respectively, and the gap distance between the electrodes was about 5 μm. As shown in Figure S1, Supporing Information in the device with the high M_w of 130 000 g mol^{-1}, the resistive switching behaviors were not observed, which is consistent with the previous study.[39] However, the devices with the low M_w of 10 000 and 23 000 g mol^{-1} clearly showed the resistive switching characteristics (see Figures S2 and S4, Supporting Information). In the organic memristors, the ECM phenomenon for resistive switching can be promoted as M_w decreased because of an increase in the free volumes for ion migration and metallization.[12] We measured the current–voltage (I–V) characteristics at six different compliance currents (CCs) (10^{-7}, 5×10^{-7}, 10^{-6}, 5×10^{-6}, 10^{-5}, and 3×10^{-5} A) to explore the ECM phenomenon for resistive switching in the device with $M_w = 10\,000\ \text{g mol}^{-1}$ (see Figure S2, Supporting Information). During the successive voltage sweeps, the CC value was set to be increased sequentially. In all the conditions, the device showed the resistive switching characteristics, and the conductance at the low resistance state (LRS) was larger at higher CCs. However, the LRS of the device was maintained only at relatively high CC conditions (10^{-5} and 3×10^{-5} A). As the CC value increased, the retention performance was enhanced, and the device exhibited a nonvolatile memory behavior in the case when the CC was larger than 10^{-5} A. When the device was operated as a nonvolatile memory, the reversible resistive switching characteristics were also observed (see Figure S3, Supporting Information). In typical ECM memristors, the conductance and memory volatility are highly dependent on the CC which governs the CF thickness,[12,42] following the results in Figure S2, Supporting Information. Moreover, in the resistive switching device with $M_w = 23\,000\ \text{g mol}^{-1}$, the nonvolatile memory characteristics were achieved at the relatively low CC conditions, compared to the device with $M_w = 10\,000\ \text{g mol}^{-1}$. For the organic ECM devices, the lateral diffusion of the CF is governed by the polymer M_w related with the free volume distributions in the medium, and thus, the memory stability is enhanced when M_w is higher.[8,12]

Let us discuss the operating principle for the resistive switching in the PVA-based memristors. Figure S5, Supporting Information shows the temperature effect on the conductance of the device with $M_w = 10\,000\ \text{g mol}^{-1}$. The LRS conductance of the device was decreased with the increase in temperature (see Figure S5, Supporting Information), which is consistent with the characteristics of the memristors based on the ECM phenomenon.[43] To clearly elucidate the physical mechanism for the resistive switching in the device, the $I - V$ curves of the device investigated via voltage sweeps with a CC of 10^{-5} A (dark blue curves in Figure S2a, Supporting Information) were replotted in a log−log scale, as shown in Figure S6, Supporting Information. During the sweeping process, the current flow followed the space charge-limited conduction composed of the regions for the Ohmic, Child's law, and abrupt conductance increase, consistent with the electrical characteristics of the ECM-based nonvolatile memory.[3,44] This means that the resistive switching behaviors in the device may be governed by the ECM mechanism.

For directly verifying the ECM phenomenon in the device, we carried out the observation of the active surface according to the resistance state, utilizing the field emission electron scanning microscopy (see Figure 1c). With the transition from the high resistance state (HRS) to the LRS, the CFs comprising several branches were formed in the active area of the device. In addition, after the erasing process, the CFs were partially ruptured. The morphology of the CFs in the device at each resistance state was similar to that of other organic ECM memristors,[45–47] indicating that the resistive switching characteristics of the PVA-based memristors originated from the ECM phenomenon consisting of the electrochemical redox reaction and the ion migration along the polymer medium.

We then developed the PVA-based transient memristor with a vertical structure, as shown in **Figure 2**a. The PVA medium with the M_w of 10 000 g mol^{-1} was used, and indium tin oxide (ITO) and silver were utilized as the inert and active electrodes, respectively. The thickness of the polymer medium (PVA) was about 300 nm. Figure 2b exhibits the I–V properties of the device. The measurement was performed at a CC of 3×10^{-5} A to obtain the nonvolatile memory characteristics, and the electroforming process was conducted to trigger the CF formation (see Figure S7, Supporting Information).[46,47] The device showed the stable nonvolatile memory performances in the bipolar mode, in accordance with the results in Figure S3, Supporting Information. The writing and erasing voltages for the device were about 1.4 and −1.0 V, respectively, and the current ratio between the HRS and the LRS was about 10^3. These operating performances are comparable with those of ECM memristors with inorganic materials.[48,49] In the previous studies, the hydroxyl groups in the thin films (about 40 nm) of PVA were aligned by an electric field, which led to the memory effect.[38,50] However, in the cases where the PVA film was relatively thick (about 300 nm), such memory effect was not observed (see Figure S8, Supporting Information). This means that the resistive switching in the device is attributed to only the metallic CF growth.

For achieving practical hardware-based neural networks, the artificial synapses of the systems should possess the stable

© 2022 The Authors. Advanced Intelligent Systems published by Wiley-VCH GmbH

26404567, 0, Downloaded from https://onlinelibrary.wiley.com/doi/10.1002/aisy.202200272 by Chung-Ang University, Wiley Online Library on [27/03/2023]. See the Terms and Conditions (https://onlinelibrary.wiley.com/terms-and-conditions) on Wiley Online Library for rules of use; OA articles are governed by the applicable Creative Commons License

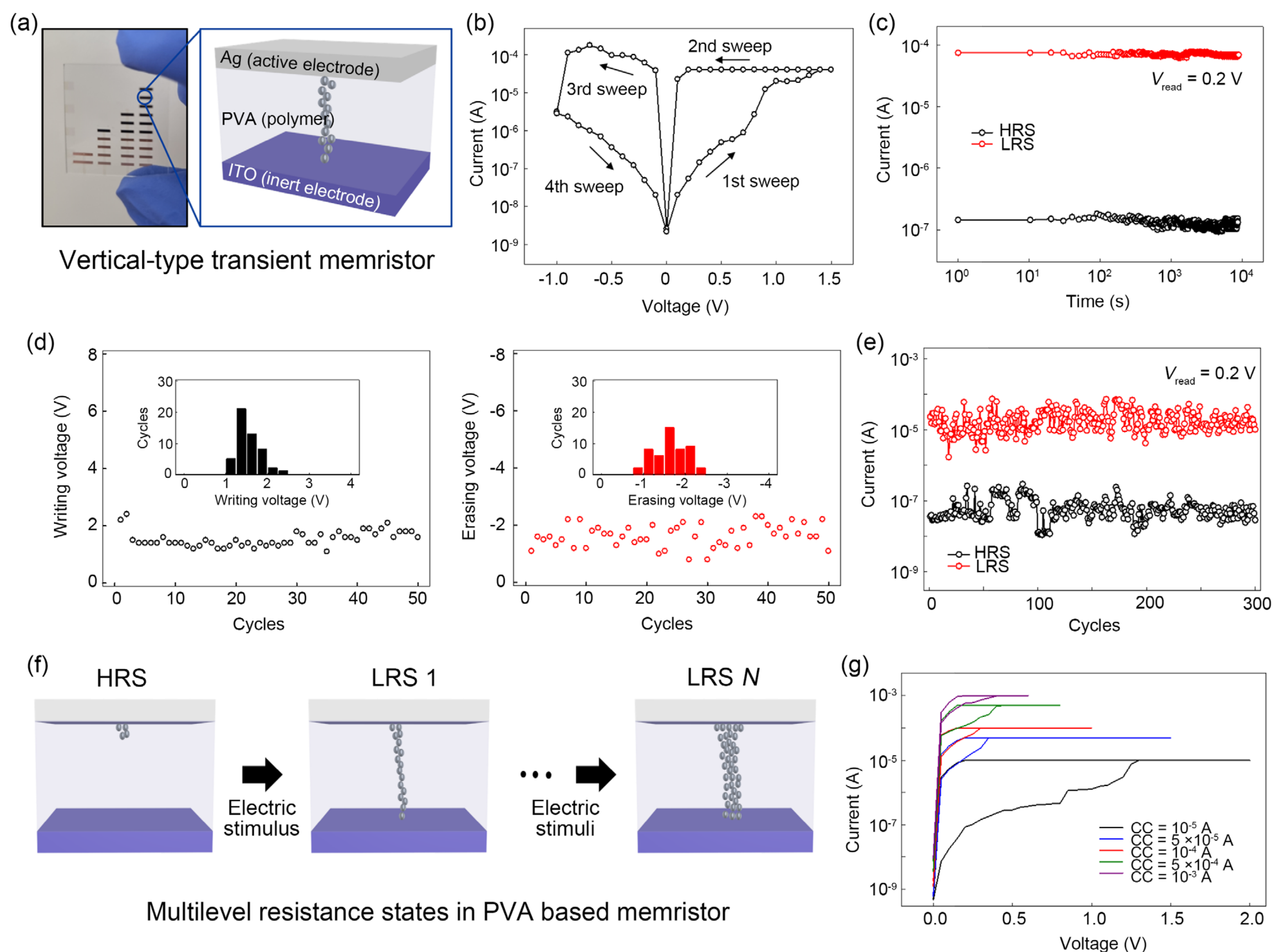

Figure 2. Characterization of the poly (vinyl alcohol)-based vertical-type memristor. a) A photographic image of the vertical-type memristor prepared on a glass substrate. An inset image illustrates the device configuration. b) Current–voltage characteristics of the device. c) Memory retention performances of the device. The read voltage (V_{read}) of 0.2 V was used in the measurements. d) Dispersions of the writing (left) and erasing (right) voltages of the device during the 50 cycles. e) Electrical durability of the device. A cycle test based on the voltage sweeps was performed, and each resistance state was checked at the V_{read} of 0.2 V. f) A schematics presenting the multilevel conductances in the device, induced by the control of the CF thickness. g) Demonstration of the multilevel conductance in the device by tuning the compliance current (CC) condition.

nonvolatile and reversible memory characteristics.[1,3] We performed a retention test for evaluating the memory stability of the developed organic memristor, as shown in Figure 2c. Each resistance state (HRS and LRS) of the device was sustained stably for 10^4 s, at a reading voltage of 0.2 V. Additionally, cycle tests for the device were performed using the repeated voltage sweeps consisting of the writing and erasing processes (see Figure 2d, e) to estimate the reproducibility of the operating voltages and the reversibility of the resistive switching. During the 50 cycles, we measured the fluctuations of the writing and erasing voltages, as shown in Figure 2d. The ratio values of the standard deviation to the average for estimating the temporal changes of the writing and erasing voltages were approximately 0.18 and 0.24, respectively. These are comparable with those of the ECM memristors with the conventional structure.[14,51,52] Note that, in the typical ECM memristors, the CF is formed in a random fashion, and it can deteriorate the reproducibility of the switching voltages.[53] Figure 2e shows the reversibility of the resistive switching in the device. The resistance of the device was stably changed by the switching processes for writing and erasing. From these stable and reversible memory performances, it can be considered that the developed organic memristor is applicable for practical neuromorphic electronics. Figure S9, Supporting Information presents the dispersions of the writing and erasing voltages for ten different cells on a single substrate. Only the small changes were observed in the switching voltages between the cells. Although the device showed the slight fluctuations at the cycle and cell-to-cell uniformity tests, the reproducibility of the switching voltages and the cell uniformity can be facilely enhanced by confining the interfacial ion injection.[54,55]

Another essential feature of memristors for artificial synapses is the multilevel state of the conductance.[1,3] We controlled the CF thickness by adjusting the CC values at the writing process, as shown in Figure 2f. The multilevel conductance was effectively demonstrated in the device (see Figure 2g), and each conductance state was maintained steadily (see Figure S10,

© 2022 The Authors. Advanced Intelligent Systems published by Wiley-VCH GmbH

26404567, 0, Downloaded from https://onlinelibrary.wiley.com/doi/10.1002/aisy.202200272 by Chung-Ang University, Wiley Online Library on [27/03/2023]. See the Terms and Conditions (https://onlinelibrary.wiley.com/terms-and-conditions) on Wiley Online Library for rules of use; OA articles are governed by the applicable Creative Commons License

Supporting Information). This implies that the developed device can be used for high-density storage systems and complex artificial neural networks. Figure S11, Supporting Information shows the effect of temperature on the conductance of the device at the LRS. The postive resistivity coefficient of the device was estimated to be about 0.0037 K^{-1}, similar to that of silver (about 0.0038 K^{-1}). This implies that the resistive switching of the vertical-type device was governed by the ECM phenomenon for the CF growth.[43] Note that the ECM memristor is a promising candidate as the highly scalable artificial synapse, because its operation is mainly governed by the localized nanoscale CF.[46,53] As shown in Figure S12, Supporting Information, our PVA-based memristor showed the stable resistive switching characteristics, irrespective of the cell area.

For the practical applications of neuromorphic systems, the synaptic device should be operated under the pulse condition.[46,47] We additionally investigated the resistive switching of the device in the pulse modes (see Figure S13, Supporting Information). The resistance state of the device was effectively controlled by the voltage pulses, and the writing and erasing times were about 5.3 and 5.0 μs, respectively. Typically, in the ECM memristors, the CF growth and the resultant resistive switching are governed by the voltage conditions.[56,57] The switching times of the device can be simply reduced by tuning the voltage amplitude.

To develop a PVA-based ECM memristor with mechanical flexibility, we fabricated the vertical-type device with $M_w = 10\,000$ $g mol^{-1}$ on a flexible substrate of polyethylene naphthalate (PEN), as shown in **Figure 3**a. Figure 3b shows the *I–V* properties of the flexible memristor at the bending states. Before the measurement, the electroforming process was performed to initiate the CF growth (see Figure S14, Supporting Information). We applied the tensile and compressive stresses to the device by conducting the negative and positive bending tests, respectively. The bending radius for the mechanical stresses was 5 mm. The stable resistive switching behaviors that are similar to those in

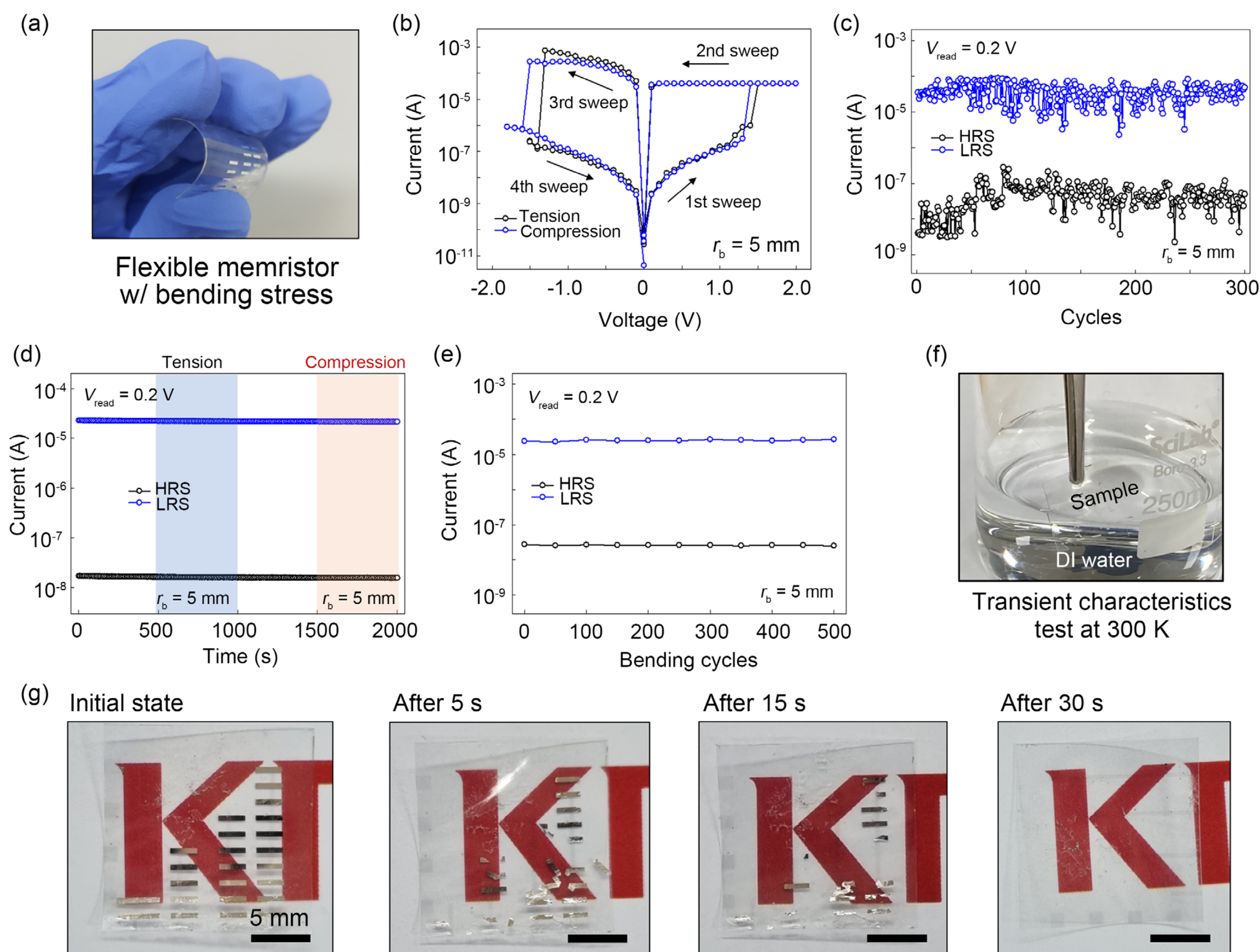

Figure 3. Electromechanical characteristics of PVA-based flexible memristors. a) A photographic image of the PVA-based flexible memristor under a mechanical stress with a bending radius (r_b) of 5 mm. b) Current–voltage characteristics of the flexible device under the bending deformations with $r_b = 5$ mm. c) Reversible memory performances of the device under the bending stress with $r_b = 5$ mm. d) Memory retention characteristics of the device investigated under the successive positive and negative bending deformations. The r_b value for each deformation was 5 mm. e) Mechanical endurance characteristics of the device. f) A photograph showing the test process for transient characteristics of the device. g) Photographic images recording the dissolution of the device in deionized water at room temperature (300 K).

© 2022 The Authors. Advanced Intelligent Systems published by Wiley-VCH GmbH

26404567, 0, Downloaded from https://onlinelibrary.wiley.com/doi/10.1002/aisy.202200272 by Chung-Ang University, Wiley Online Library on [27/03/2023]. See the Terms and Conditions (https://onlinelibrary.wiley.com/terms-and-conditions) on Wiley Online Library for rules of use; OA articles are governed by the applicable Creative Commons License

the rigid device (see Figure 3b) were observed in the flexible device at the bending states. Under the positive bending state with a radius of 5 mm, the resistance state of the device was reversibly changed from the HRS to the LRS by the repeated voltage sweeps, as shown in Figure 3c. Furthermore, the device showed the stable resistive switching behaviors under the repeated 5×10^3 pulse cycles[58] (see Figure S15, Supporting Information).

To further explore the mechanical durability of the flexible device, we investigated the effect of the repeated mechanical stresses on the memory retention performance of the device (see Figure 3d, e). As shown in Figure 3d, the positive and negative bending processes were performed sequentially in the device, during the memory retention test. The memory states (HRS and LRS) of the device were not deteriorated by the mechanical stresses, which means that the developed memristor can be used as an essential component of flexible neuromorphic systems. Figure 3e shows the results for the bending cycle tests in the device. The device showed a constant conductance at each memory state during the repeated cycles consisting of the positive and negative bending deformations with the same curvatures as those in Figure 3b. Moreover, the device was stably operated as a reversible resistive switching memory after the bending cycle tests (see Figure S16, Supporting Information). Considering that mechanical flexibility is a critical requirement for realizing wearable systems,[59] the developed memristor with high endurance for bending stresses can be useful in wearable intelligent electronics.

For confirming the transient characteristics of the developed organic memristor, we immersed the device in DI water at a room temperature of 300 K (see Figure 3f) and observed the dissolution state of the device according to the immersion time (see Figure 3g). The device was gradually dissolved in DI water and completely vanished after 30 s. This transient behavior of the device is superior to those of previously reported transient memory devices.[21–28] Note that PVA is known to be a carbon–carbon backbone polymer that is biodegradable under both aerobic and anaerobic environments.[33] In this regard, the PVA-based memristor can be used in a wide range of biodegradable neuromorphic applications.

In realizing the complex artificial neural networks with high energy efficiency, it is important to achieve the synaptic plasticity analogous to the biological counterparts in an artificial synapse[1,6,7] (see **Figure** 4a). The developed flexible memristor exhibited various synaptic functions under electric stimuli. We first measured excitatory post-synaptic current (EPSC) by applying a 10-μs voltage pulse of 1.5 V, as shown in Figure 4b. Under the voltage pulse, the conductance of the device increased and the peak current, EPSC, was observed. In addition, the device conductance decreased exponentially after removing the electric stimulus, which is analogous to the STP characteristics of a biological synapse.[60,61] To further verify the STP functions in

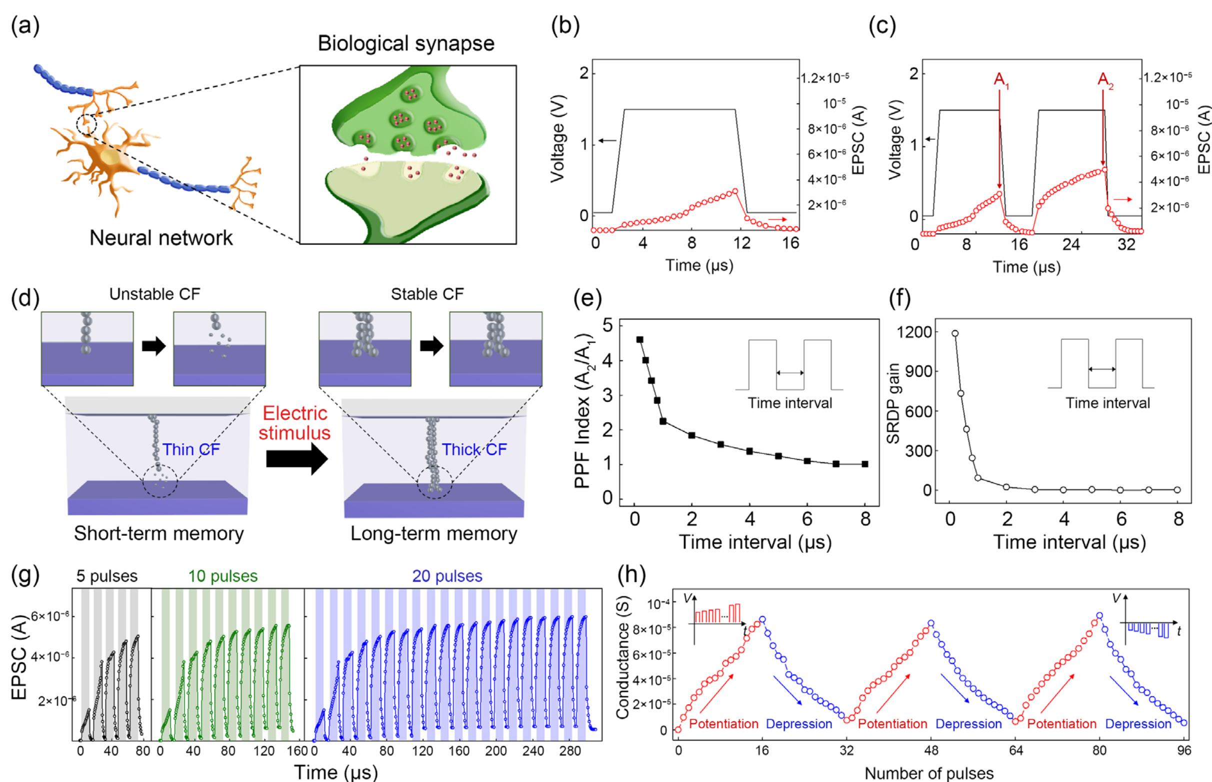

Figure 4. Synaptic characteristics of PVA-based flexible memristors. a) Schematics illustrating biological neural networks consisting of synapses. b) Excitatory post-synaptic current (EPSC) under electric stimulus. c) Paired-pulse facilitation (PPF) by two successive voltage pulses (the width and interval for pulses were 10 and 4 μs, respectively). d) Schematics showing a principle for achieving synaptic plasticity in the organic memristor. e) PPF index as a function of a time interval value between two successive voltage pulses (1.5 V, 10 μs). f) Spike-rate-dependent plasticity. g) Spike-number-dependent plasticity under the repeated voltage pulses (1.5 V, 10 μs). h) Multilevel memory states of the device achieved in the pulse mode.

© 2022 The Authors. Advanced Intelligent Systems published by Wiley-VCH GmbH

26404567, 0, Downloaded from https://onlinelibrary.wiley.com/doi/10.1002/aisy.202200272 by Chung-Ang University, Wiley Online Library on [27/03/2023]. See the Terms and Conditions (https://onlinelibrary.wiley.com/terms-and-conditions) on Wiley Online Library for rules of use; OA articles are governed by the applicable Creative Commons License

the flexible memristor, two successive 1.5-V voltage pulses separated by a time interval of 4 μs were applied to the device (see Figure 4c). The EPSC was larger at the second pulse (A_2) than at the first pulse (A_1), implying the demonstration of PPF, a STP property, in the device. Typically, for the ECM memristors consisting of an insulating layer without any dopant, the lateral diffusion of the metal atoms, and the resultant self-dissolution of the CF are facilitated in the immature filament, which results in the volatile memory characteristics.[12,16] When the electric stimulus is not sustained sufficiently to grow the CF stably, the developed device exhibits the short-term memory characteristics. In addition, the short-term memory state of the device can be transited to the long-term memory state by an additional electric stimulus, before the unstable CF has been disrupted completely (see Figure 4d). As shown in Figure S17, Supporting Information, the device showed the volatile memory characteristics under the relatively short pulse condition; however, the device was operated as a nonvolatile memory at the longer voltage pulse. Figure 4e shows a PPF index estimated as A_2/A_1, according to a time interval between the applied voltage pulses. As the interval decreased from 8.0 to 0.2 μs, the PPF index increased from 1.01 to 4.61, being an indicative of the stable STP properties of the device.[62,63] Furthermore, we confirmed that the time window of synaptic plasticity can be effectively tuned by the PVA M_w, the diffusive parameter for the CF in the device,[8] as shown in Figure S18, Supporting Information. As M_w increased, the CF stability and PPF index were enhanced, indicating a slower time window for the synaptic plasticity of the PVA-based synapse.

We also investigated SRDP and SNDP, the important spike-dependent learning rules in a brain,[7,62] in the flexible device (see Figure 4f,g). For SRDP, two consecutive 1.5-V voltage pulses with 10 μs were applied to the device, and the SRDP gain, a ratio of the increased conductance value to the initial conductance, was measured with different time interval conditions for the applied voltage pulses. Decrease in a time interval from 8.0 to 0.2 μs, induced an increase in the SRDP gain from 1.05 to 1188.62. Moreover, the EPSC response and the device conductance were effectively tuned through the voltage pulse number (see Figure 4g). With the pulse number, the EPSC value and the device conductance increased. Note that the non-linear increase in the device conductance is attributed to the abrupt growth of the CF, which is similar to the typical ECM memristors.[13]

For mimicking the reliable memory states of biological synapses, we controlled the device conductance by utilizing the varying electric stimuli, as shown in Figure 4h. In the potentiation process, the voltage pulse with 20 μs was gradually increased from 1.10 to 1.58 V. For the depression process, the amplitude of the 20-μs pulse was decreased from −1.00 to −1.48 V. Under such pulse conditions, the device clearly exhibited the multilevel memory states consisting of 16 different conductance levels. It should be noted that, in ECM memristors, voltage pulses with gradually varying amplitudes are ideal electric stimuli for controlling the conductance linearly.[12] Table S2, Supporting Information shows the electrical performances and synaptic characteristics of the transient memristors previously reported.[20–30] Although the previous memristors based on various structures exhibited resistive switching characteristics, the synaptic plasticity has not been completely replicated in the devices so far. Based on the optimized synaptic plasticity demonstrated in the developed flexible device, it can be thought that the PVA-based memristor is suitable and ideal for spike-dependent neuromorphic computing applications with high energy efficiency.

For realizing practical neuromorphic systems, parallel computation in synapse arrays is an essential requirement.[64–66] To evaluate the potentials of the device for parallel computation with spike-dependent learning process, we prepared the multicells of the developed memristors acting as an artificial synapse, as shown in **Figure 5**a. The memristor cells were then trained for logic operators of OR and AND (see Figure 5b), and the consumed energy values for the training and computing processes were ananlyzed, as shown in Figure S19, Supporting Information. In training the system, the SRDP characteristics of the cell were used for high energy efficiency and a simple scheme (see Figure S20, Supporting Information). For the learning processes of "OR" and "AND," the developed system consumed approximately 4.28 and 1.01 nJ, respectively. For each logic operation, a single layer consisting of two input neurons and one output neuron was connected by two synapses. In the logic operators, two different binary inputs (V_1 and V_2) with the pulse width of 100 ns were used, and an output current (I_{OR} for OR and I_{AND} for AND) was checked for a logic output. For logic inputs, 0.2 V and 0.002 V were utilized for "1" and "0," respectively, and the measured output current was compared with a threshold current (I_{th}) of 9 μA to estimate the output value. When the output current was higher (or lower) than 9 μA, the logic output was determined as "1" (or "0"). The memristor cells were reliably operated as the logic operators, as shown in Figure 5c. The average operating energy for the "OR" and "AND" logic computing was about 241 fJ, which is superior to that in CMOS systems.[67] Furthermore, we prepared the synapse array consisting of the 15 different memristor cells to achieve the complex logic operations. To store the letters of "K," "N," "U," "A," and "I" in the synapse array according to American standard code for information interchange (ASCII) based on the octal numbers, each cell was utilized as a synaptic component with nine different memory states. The spike-dependent learning processes for the letters (see Figure S21, Supporting Information) were effectively performed by consuming about 8.49 nJ, and the computing operation for the stored letters was reliably achieved at a 0.2-V reading voltage with 100 ns, with about 149 fJ (see Figure 5d). This indicates that our memristor can be utilized as an artificial synapse for energy efficient hardware neural networks.

In general, the performances of the artificial neural networks can be evaluated through their recognition capability for several types of pattern images.[68–70] To confirm the capability of the developed PVA-based memristor for constructing the complex neural network, we conducted the numerical simulation of SPICE for the handwritten digit pattern recognition based on a data set of the Modified National Institute of Standards and Technology (MNIST),[71,72] as shown in Figure 5e. In the simulation, 60 000 images for learning and 10 000 images for classifying tests were utilized, and the pixel of each image had 256 levels for grayscale. A neural network was simply composed of a single layer, and 784 and 10 neurons were set for the digit

© 2022 The Authors. Advanced Intelligent Systems published by Wiley-VCH GmbH

26404567, 0, Downloaded from https://onlinelibrary.wiley.com/doi/10.1002/aisy.202200272 by Chung-Ang University, Wiley Online Library on [27/03/2023]. See the Terms and Conditions (https://onlinelibrary.wiley.com/terms-and-conditions) on Wiley Online Library for rules of use; OA articles are governed by the applicable Creative Commons License

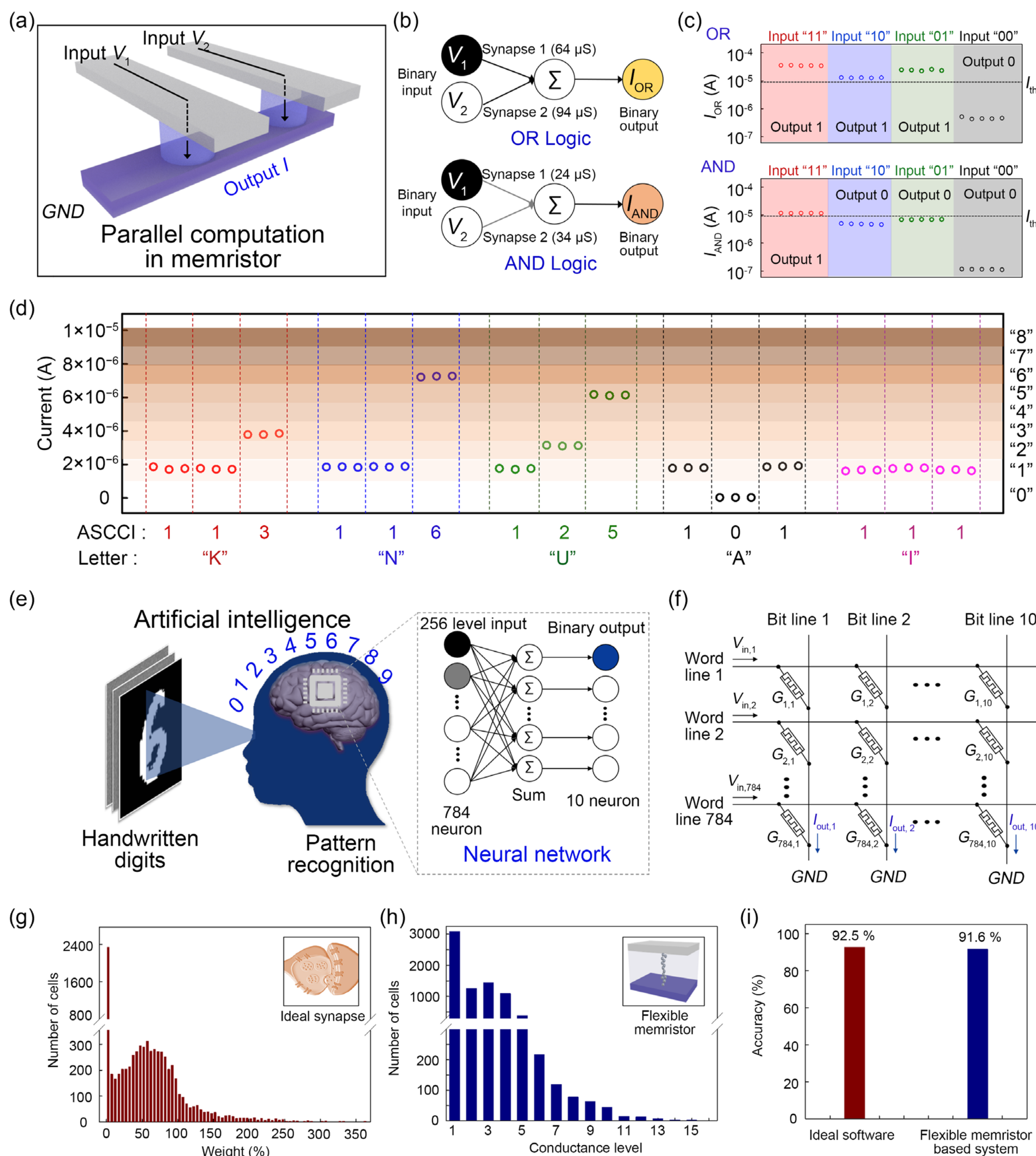

Figure 5. An artificial intelligence system based on the developed flexible memristor. a) A schematic of parallel computation in memristor arrays. b) Diagram of the trained neural network based on the developed memristor for logic operations of OR and AND. c) Parallel computation for AND and OR utilizing the developed synapse cells. d) The letters of "K," "N," "U," "A," and "I" displayed in the parallel connected synapse cells, according to the ASCII code based on the octal numbers. Each letter was confirmed at a 0.2-V reading voltage with 100 ns. e) A schematic presenting a configuration of the hardware-based neural network for recognizing the handwritten digit images. f) A schematic diagram showing the crossbar array of the developed flexible memristor for the neural network. g) Synaptic weight distribution that was calculated in the ideal software system for recognizing the handwritten digits. h) Conductance distribution of the developed memristor array after the training process for the recognition of the handwritten digits. i) The pattern recognition accuracy after the learning processes for 50 epochs in the ideal software system and the hardware-based neural network consisting of the developed flexible memristor.

images of 28 × 28 pixels and the classes of the digit images, respectively. The input and output neurons were connected through a single flexible memristor device, as shown in Figure 5f. In the learning processes, the ideal weight distribution calculated in the software system for classifying the digit images for MNIST (see Figure 5g) was converted to the cell conductance in the device arrays. It should be noted that the conductance parameters of the device cell were obtained from the results in Figure 4h. Only positive weight values were utilized to facilely convert the synaptic weight to the device conductance. Figure 5h

© 2022 The Authors. Advanced Intelligent Systems published by Wiley-VCH GmbH

26404567, 0, Downloaded from https://onlinelibrary.wiley.com/doi/10.1002/aisy.202200272 by Chung-Ang University, Wiley Online Library on [27/03/2023]. See the Terms and Conditions (https://onlinelibrary.wiley.com/terms-and-conditions) on Wiley Online Library for rules of use; OA articles are governed by the applicable Creative Commons License

shows the conductance distribution of the memristor array after the learning processes for 50 epochs. The ideal synaptic weights consisting of analog memory states were effectively quantized to the 16 levels of the device conductance. For the process of the recognition tests, the 0.1-V input voltage with 100 ns was applied to each cell, and the output current values of bit lines were confirmed. In the neural network based on the developed memristor, the pattern recognition accuracy was about 92% after training 50 epochs, which is highly close to that of the ideal software system (see Figure 5i). In addition, when the current-sensing resistor of 1 mΩ was utilized, the developed hardware neural networks classified digit images by consuming about 255 pJ, which is greatly more efficient than that of the von Neumann counterparts.[70] This implies that the developed PVA-based memristor with biodegradability and mechanical flexibility can be used as a synaptic device in the energy efficient hardware neural networks with high integration density.

3. Conclusion

In conclusion, we demonstrated a biodegradable and flexible polymer-based memristor with optimized synaptic plasticity for the spike-dependent learning process. We explored the ECM phenomenon and the resultant CF growth in the pure PVA medium and analyzed the resistive switching effect of the PVA-based memristor. It was found that, in the PVA-based memristors, the metallic CF growth and its stability were effectively tuned by the polymer M_w. The developed PVA-based memristor was stably operated as a resistive switching memory device, and the multilevel conductance states were effectively achieved by tuning the applied voltage conditions including the CC and the amplitude. The PVA-based memristor prepared on the plastic substrate exhibited the high mechanical flexibility and endurance performances, which is important for practical wearable electronics. Additionally, the developed flexible memristor was also acted as a transient device with highly superior biodegradability due to the high water solubility of the PVA medium. Moreover, the device showed the reliable synaptic characteristics and the applicability as an artificial synapse for the energy efficient neural networks. The simple and complex logic operators were effectively trained in the developed synapse arrays through the spike-dependent learning process with low-energy consumption. Furthermore, the intelligent system with high energy efficiency for recognizing the handwritten digits was effectively constructed by utilizing the developed device, and such system exhibited the high pattern recognition accuracy of about 92% which is close to that of the ideal software neural network. This novel strategy of realizing a transient and flexible synaptic device with the spike-dependent operation would be a fundamental platform for developing eco-friendly smart wearable electronics that are linked to next-generation intelligent systems.

4. Experimental Section

Characterization: The film thickness of the device was measured using a profiler (DektakXT-A, Bruker). The electrical characteristics of the devices were measured using a semiconductor parameter analyzer (4200-SCS, Keithley) combined with an ultrafast *I–V* module (4225-PMU, Keithley), in an ambient condition with a relative humidity of 30%, at 27 °C. In the electrical measurements, the inert electrode (gold or ITO) was grounded, and the active electrode of silver was used for the scanning voltage. The active area of the lateral-type memristor was investigated using a field-emission scanning electron microscope (S-4800, Hitachi).

Fabrication of the Organic Memristors with a Planar Structure: To fabricate an organic memristor with a planar structure, a glass substrate was cleaned under ultrasonication in acetone, isopropyl alcohol, and deionized water in sequence for 10 min. For the inert electrode, a 50-nm-thick gold layer was thermally deposited on the substrate at 1 Å s^{-1} under 10^{-6} Torr. The inert electrode was patterned using a photoresist (PR) (AZ 1512, AZ electronic materials) through conventional photolithography and a wet-etching process using an etchant (TFA, Transene) for gold. Then, the active electrode of 50-nm-thick silver was thermally evaporated on the PR-patterned film at 1 Å s^{-1} under 10^{-6} Torr. Through the lift-off process for removing the PR, the active electrode was patterned. The width of each electrode and the gap distance between the electrodes were about 300 and 5 μm, respectively. As the polymer medium, a poly (vinyl alcohol) (PVA) powder with molecular weight (M_w) of 10 000, 23 000, or 130 000 $gmol^{-1}$, dissolved in deionized water in 5, 4, or 2 wt%, respectively, was spin-coated on the substrate with the electrode patterns, at a rate of 2000 rpm for 30 s. The PVA layer was soft-baked at 100 °C for 1 h to remove the residual solvent after spin-coating.

Fabrication of the Organic Memristor with a Vertical Structure: To fabricate an organic memristor with a vertical structure, an ITO-patterned substrate (glass for a rigid device and polyethylene naphthalate for a flexible device) was cleaned under ultrasonication in acetone, isopropyl alcohol, and deionized water sequentially for 10 min. Note that the ITO patterns on the substrate acted as inert electrodes of the memristors. Regarding the polymer medium of the devices, PVA, with $M_w = 10\,000$ $gmol^{-1}$ (or 13 000 $gmol^{-1}$), dissolved in deionized water in 5 wt% (or 4 wt%) was spin-coated on the substrate at a rate of 2000 rpm for 30 s. The PVA layer was then annealed at 100 °C for 1 h. The thickness of the PVA film was about 300 nm. For producing the active electrode, a 50-nm-thick silver layer was thermally evaporated at 1 Å s^{-1} under 10^{-6} Torr. The active area of the devices was 0.5×0.5 mm^2.

Supporting Information

Supporting Information is available from the Wiley Online Library or from the author.

Acknowledgements

S.O. and H.K. contributed equally to this work. This work was supported by the National Research Foundation of Korea (NRF) under grant funded by the Korea Government (MSIT) (2020R1F1A1075436). This research was supported by National R&D Program through the National Research Foundation of Korea (NRF) funded by Ministry of Science and ICT (2021M3F3A2A03017764). This research was supported by the BK21 FOUR project funded by the Ministry of Education, Korea (4199990113966). This work was supported by the National Research Foundation of Korea (NRF) grant funded by the Korea government (Ministry of Science and ICT) (No. 2021R1C1C2012074). This work was also supported by the National Research Foundation of Korea (NRF) grant funded by the Korea government (MIST) (NRF-2022R1C1C100923511).

Conflict of Interest

The authors declare no conflict of interest.

© 2022 The Authors. Advanced Intelligent Systems published by Wiley-VCH GmbH

26404567, 0, Downloaded from https://onlinelibrary.wiley.com/doi/10.1002/aisy.202200272 by Chung-Ang University, Wiley Online Library on [27/03/2023]. See the Terms and Conditions (https://onlinelibrary.wiley.com/terms-and-conditions) on Wiley Online Library for rules of use; OA articles are governed by the applicable Creative Commons License

Data Availability Statement

The data that support the findings of this study are available from the corresponding author upon reasonable request.

Keywords

artificial synapses, flexible memristors, neural networks, synaptic function, transient memristors

Received: August 19, 2022
Revised: October 15, 2022
Published online:

[1] Y. van de Burgt, A. Melianas, S. T. Keene, G. Malliaras, A. Salleo, *Nat. Electron.* **2018**, *1*, 386.
[2] X. Feng, Y. Li, L. Wang, S. Chen, Z. G. Yu, W. C. Tan, N. Macadam, G. Hu, L. Huang, L. Chen, X. Gong, D. Chi, T. Hasan, A. V.-Y. Thean, Y.-W. Zhang, K.-W. Ang, *Adv. Electron. Mater.* **2019**, *5*, 1900740.
[3] M.-H. Kim, H.-L. Park, M.-H. Kim, J. Jang, J.-H. Bae, I. M. Kang, S.-H. Lee, *npj Flex. Electron.* **2021**, *5*, 34.
[4] S. Lequeux, J. Sampaio, V. Cros, K. Yakushiji, A. Fukushima, R. Matsumoto, H. Kubota, S. Yuasa, J. Grollier, *Sci. Rep.* **2016**, *6*, 31510.
[5] Y. Sun, N. He, D. Wen, F. Sun, *Appl. Surf. Sci.* **2021**, *564*, 150452.
[6] B. Bannur, B. Yadav, G. U. Kulkarni, *ACS Appl. Electron. Mater.* **2022**, *4*, 1552.
[7] H.-L. Park, Y. Lee, N. Kim, D.-G. Seo, G.-T. Go, T.-W. Lee, *Adv. Mater.* **2020**, *32*, 1903558.
[8] S.-H. Lee, H.-L. Park, M.-H. Kim, M.-H. Kim, B.-G. Park, S.-D. Lee, *ACS Appl. Mater. Interfaces* **2020**, *12*, 51719.
[9] H.-L. Park, T.-W. Lee, *Org. Electron.* **2021**, *98*, 106301.
[10] N. Raeis-Hosseini, Y. Park, J.-S. Lee, *Adv. Funct. Mater.* **2018**, *28*, 1800553.
[11] P.-P. Lu, J.-X. Shen, D.-S. Shang, Y. Sun, *ACS Appl. Mater. Interfaces* **2020**, *12*, 4673.
[12] S.-H. Lee, H.-L. Park, C.-M. Keum, I.-H. Lee, M.-H. Kim, S.-D. Lee, *Phys. Status Solidi RRL* **2019**, *13*, 1900044.
[13] B. C. Jang, S. Kim, S. Y. Yang, J. Park, J.-H. Cha, J. Oh, J. Choi, S. G. Im, V. P. Dravid, S.-Y. Choi, *Nano Lett.* **2019**, *19*, 839.
[14] H.-L. Park, M.-H. Kim, S.-H. Lee, *Adv. Electron. Mater.* **2020**, *6*, 2000582.
[15] Z. Wang, S. Joshi, S. E. Savel'ev, H. Jiang, R. Midya, P. Lin, M. Hu, N. Ge, J. P. Strachan, Z. Li, Q. Wu, M. Barnell, G.-L. Li, H. L. Xin, R. S. Williams, Q. Xia, J. Joshua Yang, *Nat. Mater.* **2017**, *16*, 101.
[16] Q. Hua, H. Wu, B. Gao, M. Zhao, Y. Li, X. Li, X. Hou, M.-F. Chang, P. Zhou, H. Qian, *Adv. Sci.* **2019**, *6*, 1900024.
[17] K. K. Fu, Z. Wang, J. Dai, M. Carter, L. Hu, *Chem. Mater.* **2016**, *28*, 3527.
[18] Y. Gao, Y. Zhang, X. Wang, K. Sim, J. Liu, J. Chen, X. Feng, H. Xu, C. Yu, *Sci. Adv.* **2017**, *3*, 1701222.
[19] S. G. Sarwat, B. Kersting, T. Moraitis, V. P. Jonnalagadda, A. Sebastian, *Nat. Nanotechnol.* **2022**, *17*, 507.
[20] N. R. Hosseini, J.-S. Lee, *Adv. Funct. Mater.* **2015**, *25*, 5586.
[21] X. He, J. Zhang, W. Wang, W. Xuan, X. Wang, Q. Zhang, C. G. Smith, J. Luo, *ACS Appl. Mater. Interfaces* **2016**, *8*, 10954.
[22] H. Wang, B. Zhu, X. Ma, Y. Hao, X. Chen, *Small* **2016**, *12*, 2715.
[23] S. Wu, H. Wang, J. Sun, F. Song, Z. Wang, M. Yang, H. Xi, Y. Xie, H. Gao, J. Ma, X. Ma, Y. Hao, *IEEE Electron Device Lett.* **2016**, *37*, 990.
[24] J. Sun, H. Wang, F. Song, Z. Wang, B. Dang, M. Yang, H. Gao, X. Ma, Y. Hao, *Small* **2018**, *14*, 1800945.
[25] F. Song, H. Wang, J. Sun, H. Gao, S. Wu, M. Yang, X. Ma, Y. Hao, *IEEE Electron Device Lett.* **2019**, *39*, 31.
[26] X. Ji, L. Song, S. Zhong, Y. Jiang, K. G. Lim, C. Wang, R. Zhao, *J. Phys. Chem. C* **2018**, *122*, 16909.
[27] J. Xu, X. Zhao, Z. Wang, H. Xu, J. Hu, J. Ma, Y. Liu, *Small* **2019**, *15*, 1803970.
[28] Q. Lin, S. Hao, W. Hu, M. Wang, Z. Zang, L. Zhu, J. Du, X. Tang, *J. Mater. Chem. C* **2019**, *7*, 3315.
[29] Y. Guo, W. Hu, F. Zeng, C. Zhang, Y. Peng, Y. Guo, *Org. Electron.* **2020**, *83*, 105750.
[30] B. Sueoka, F. Zhao, *J. Phys. D: Appl. Phys.* **2022**, *55*, 225105.
[31] A. Dorigato, A. Pegoretti, *Colloid Polym. Sci.* **2012**, *290*, 359.
[32] H. Ahmed, A. Hashim, *Silicon* **2021**, *13*, 2639.
[33] Z. Zhang, C. Du, H. Jiao, M. Zhang, *Adv. Electron. Mater.* **2020**, *6*, 1901133.
[34] X. Wang, X. Wang, M. Pi, R. Ran, *Chem. Eng. J.* **2022**, *428*, 131172.
[35] J. J. L. Hmar, *RSC Adv.* **2018**, *8*, 20423.
[36] T. Kim, D.-K. Kim, J. Kim, J. J. Pak, *Semicond. Sci. Technol.* **2019**, *34*, 065006.
[37] H. H. Nguyen, H. K. T. Ta, S. Park, T. B. Phan, N. K. Pham, *RSC Adv.* **2020**, *10*, 12900.
[38] Y. Lei, Y. Liu, Y. Xia, X. Gao, B. Xu, S. Wang, J. Yin, Z. Liu, *AIP Adv.* **2014**, *4*, 077105.
[39] K. Krishnan, M. Aono, T. Tsuruoka, *J. Mater. Chem. C* **2018**, *6*, 6460.
[40] Y. Park, J.-S. Lee, *ACS Appl. Mater. Interfaces* **2021**, *13*, 1021.
[41] K. S. Woo, J. Kim, J. Han, J. M. Choi, W. Kim, C. S. Hwang, *Adv. Intell. Syst.* **2021**, *3*, 2100062.
[42] C.-P. Hsiung, H.-W. Liao, J.-Y. Gan, T.-B. Wu, J.-C. Hwang, F. Chen, M.-J. Tsai, *ACS Nano* **2010**, *4*, 5414.
[43] B. C. Jang, H. Seong, S. K. Kim, J. Y. Kim, B. J. Koo, J. Choi, S. Y. Yang, S. G. Im, S.-Y. Choi, *ACS Appl. Mater. Interfaces* **2016**, *8*, 12951.
[44] Y. Sun, C. Song, J. Yin, X. Chen, Q. Wan, F. Zeng, F. Pan, *ACS Appl. Mater. Interfaces* **2017**, *9*, 34064.
[45] H.-L. Park, M.-H. Kim, S.-H. Lee, *Org. Electron.* **2020**, *87*, 105927.
[46] H.-L. Park, M.-H. Kim, M.-H. Kim, S.-H. Lee, *Nanoscale* **2020**, *12*, 22502.
[47] H.-L. Park, M.-H. Kim, H. Kim, S.-H. Lee, *Adv. Electron. Mater.* **2021**, *7*, 2100299.
[48] J. Lee, J.-H. Ryu, B. Kim, F. Hussain, C. Mahata, E. Sim, M. Ismail, Y. Abbas, H. Abbas, D. K. Lee, M.-H. Kim, Y. Kim, C. Choi, B.-G. Park, S. Kim, *ACS Appl. Mater. Interfaces* **2020**, *12*, 33908.
[49] Z. Wang, B. Sun, H. Ye, Z. Liu, G. Liao, T. Shi, *Appl. Surf. Sci.* **2021**, *546*, 149094.
[50] T.-D. Tsai, J.-W. Chang, T.-C. Wen, T.-F. Guo, *Adv. Funct. Mater.* **2013**, *23*, 4206.
[51] W. Ding, Y. Tao, X. Li, Y. Lin, Z. Wang, H. Xu, X. Zhao, W. Liu, J. Ma, Y. Liu, *Phys. Status Solidi RRL* **2018**, *12*, 1800285.
[52] P. T. Chandane, T. D. Dongale, P. B. Patil, A. P. Tiwari, *J. Mater. Sci.: Mater. Electron.* **2019**, *30*, 21288.
[53] S. Choi, S. H. Tan, Z. Li, Y. Kim, C. Choi, P.-Y. Chen, H. Yeon, S. Yu, J. Kim, *Nat. Mater.* **2018**, *17*, 335.
[54] Q. Liu, S. Long, H. Lv, W. Wang, J. Niu, Z. Huo, J. Chen, M. Liu, *ACS Nano* **2010**, *4*, 6162.
[55] S.-H. Lee, H.-L. Park, M.-H. Kim, S. Kang, S.-D. Lee, *ACS Appl. Mater. Interfaces* **2019**, *11*, 30108.
[56] R. Waser, R. Dittmann, G. Staikov, K. Szot, *Adv. Mater.* **2009**, *21*, 2632.
[57] I. Valov, R. Waser, J. R. Jameson, M. N. Kozicki, *Nanotechnology* **2011**, *22*, 254003.
[58] M. Lanza, R. Waser, D. Ielmini, J. J. Yang, L. Goux, J. Suñe, A. J. Kenyon, A. Mehonic, S. Spiga, V. Rana, S. Wiefels, S. Menzel, I. Valov, M. A. Villena, E. Miranda, X. Jing, F. Campabadal, M. B. Gonzalez, F. Aguirre, F. Palumbo, K. Zhu, J. B. Rolan,

© 2022 The Authors. Advanced Intelligent Systems published by Wiley-VCH GmbH

26404567, 0, Downloaded from https://onlinelibrary.wiley.com/doi/10.1002/aisy.202200272 by Chung-Ang University, Wiley Online Library on [27/03/2023]. See the Terms and Conditions (https://onlinelibrary.wiley.com/terms-and-conditions) on Wiley Online Library for rules of use; OA articles are governed by the applicable Creative Commons License

F. M. Puglisi, L. Larcher, T.-H. Hou, T. Prodromakis, Y. Yang, P. Huang, T. Wan, Y. Chai, et al., *ACS Nano* **2021**, *15*, 17214.
[59] C. Zhu, E. Chalmers, L. Chen, Y. Wang, B. B. Xu, Y. Li, X. Liu, *Small* **2019**, *15*, 1902440.
[60] P. A. Salin, M. Scanziani, R. C. Malenka, R. A. Nicoll, *Proc. Natl. Acad. Sci. U.S.A.* **1996**, *93*, 13304.
[61] H.-L. Park, H. Kim, D. Lim, H. Zhou, Y.-H. Kim, Y. Lee, S. Park, T.-W. Lee, *Adv. Mater.* **2020**, *32*, 1906899.
[62] J. Lao, W. Xu, C. Jiang, N. Zhong, B. Tian, H. Lin, C. Luo, J. Travas-sejdic, H. Peng, C.-G. Duan, *J. Mater. Chem. C* **2021**, *9*, 5706.
[63] S.-R. Zhang, L. Zhou, J.-Y. Mao, Y. Ren, J.-Q. Yang, G.-H. Yang, X. Zhu, S.-T. Han, V. A. L. Roy, Y. Zhou, *Adv. Mater. Technol.* **2019**, *4*, 1800342.
[64] D. Ielmini, H.-S. Philip Wong, *Nat. Electron.* **2018**, *1*, 333.
[65] V. Joshi, M. L. Gallo, S. Haefeli, I. Boybat, S. R. Nanakumar, C. Piveteau, M. Dazzi, B. Rajendran, A. Sebastian, E. Eleftheriou, *Nat. Commun.* **2020**, *11*, 2473.
[66] P. Yao, H. Wu, B. Gao, J. Tang, Q. Zhang, W. Zhang, J. Joshua Yang, H. Qian, *Nature* **2020**, *577*, 641.
[67] S. E. Kim, M.-H. Kim, J. Jang, H. Kim, S. Kim, J. Jang, J.-H. Bae, I. M. Kang, S.-H. Lee, *Adv. Intell. Syst.* **2022**, *4*, 2200110.
[68] X. Feng, S. Li, S. L. Wong, S. Tong, L. Chen, P. Zhang, L. Wang, X. Fong, D. Chi, K.-W. Ang, *ACS Nano* **2021**, *15*, 1764.
[69] S. Kim, K. Heo, S. Lee, S. Seo, H. Kim, J. Cho, H. Lee, K.-B. Lee, J.-H. Park, *Nanoscale Horiz.* **2021**, *6*, 139.
[70] A. Shrestha, H. Fang, D. P. Rider, Z. Mei, Q. Qiu, in *Proc. of DAC*, IEEE, San Francisco, CA **2021**, pp. 367–372.
[71] S. Kim, J. Chen, Y.-C. Chen, M.-H. Kim, H. Kim, M.-W. Kwon, S. Hwang, M. Ismail, Y. Li, X.-S. Miao, Y.-F. Chang, B.-G. Park, *Nanoscale* **2019**, *11*, 237.
[72] Z. Wang, Q. Zheng, J. Kang, Z. Yu, G. Zhong, Y. Ling, L. Bao, S. Bao, G. Bai, S. Zheng, Y. Cai, J. Robertson, R. Huang, *IEEE Trans. Electron Devices* **2020**, *67*, 4166.

 © 2022 The Authors. Advanced Intelligent Systems published by Wiley-VCH GmbH

26404567, 0, Downloaded from https://onlinelibrary.wiley.com/doi/10.1002/aisy.202200272 by Chung-Ang University, Wiley Online Library on [27/03/2023]. See the Terms and Conditions (https://onlinelibrary.wiley.com/terms-and-conditions) on Wiley Online Library for rules of use; OA articles are governed by the applicable Creative Commons License